DOI: 10.1021/cg901355c

CRYSTAL GROWTH & DESIGN Article

2010, Vol. 10
1725–1729

Epitaxial Structure of (001)- and (111)-Oriented Perovskite Ferrate Films Grown by Pulsed-Laser Deposition

Suvankar Chakraverty,[†] Akira Ohtomo,*[,†] Masaki Okude,[†] Kazunori Ueno,[‡] and Masashi Kawasaki[†,‡,§]

[†]*Institute for Materials Research, Tohoku University, 2-1-1 Katahira, Aoba-ku, Sendai 980-8577, Japan,* [‡]*WPI Advanced Institute for Materials Research, Tohoku University, 2-1-1 Katahira, Aoba-ku, Sendai 980-8577, Japan, and CREST,* [§]*Japan Science and Technology Agency, 5 Sanbancho, Chiyoda-ku, Tokyo 102-0075, Japan*

Received October 30, 2009; Revised Manuscript Received February 4, 2010

ABSTRACT: We report epitaxial growth and structures of $SrFeO_{2.5}$ (SFO) films on $SrTiO_3$ (STO) (001) and (111) substrates by pulsed-laser deposition. Reflection high-energy electron diffraction intensity oscillations were observed during the initial growth on both substrates, reflecting a layer-by-layer growth mode of the formula unit cell. It was found that the films were stabilized with a monoclinic structure that was derived from the original orthorhombic structure of bulk Brownmillerite. Using an X-ray reciprocal space mapping technique, in-plane domain structures and the orientation relationship were investigated. In addition, the impact of laser spot area on the epitaxial structures was studied. For the films grown on the (001) STO, the orientation relationship was robust against the change of the laser spot area: SFO(001)//STO(001) and SFO(100)//STO(100) for the out-of-plane and the in-plane, respectively, with the [001] axis tilted toward the 4-fold *a*- and *b*-axes by ~1.4°, whereas nearly (111)-oriented films were obtained on the (111) STO, exhibiting a complicated manner of tilting that depended on laser spot area. The observed variation in tilting configurations can be understood in terms of possible atomic arrangements at the SFO/STO interface. These results present a guide to control the heteroepitaxial growth and structure of (111)-oriented noncubic perovskites.

1. Introduction

Perovskite oxides exhibit a wide variety of physical properties, including superconductivity, ferroelectricity, and magnetism.[1] The possibility of coherent integration of the functions present in their rich ground states has prompted us to explore the growth of artificial superlattices that may exhibit even a wider variety of the properties than the bulk. Most of the previous attempts have been made with (001)-orientated films,[2] whereas there has been very limited success on the growth of (111)-oriented superlattices, perhaps due to lack of our understanding of the epitaxial growth mechanism. More generally, it is not necessarily guaranteed that the properties of epitaxial films grown along the (111) direction are the same as those of bulk or (001)-oriented films, which is a key point to explore in a new class of superlattices such as double perovskites.[3]

Pulsed-laser deposition (PLD) is regarded as one of the best methods to grow high-quality complex oxide thin films and has been widely applied for the heteroepitaxial growth of the perovskite oxides.[4] PLD has many growth parameters, which need to be optimized to get the desired materials properties. In addition, a careful study on a model system is essential to know how the structural and physical properties of a material change as a function of growth direction under the same growth conditions.

To pursue the research aimed at this purpose, we choose a perovskite ferrate compound, $SrFeO_{3-\delta}$, which exhibits a wide variety of physical properties and structures that depend strongly on oxygen stoichiometry. Under ambient conditions, the crystalline symmetry varies with increasing δ; cubic $SrFeO_3$ ($\delta = 0$), tetragonal $Sr_8Fe_8O_{23}$ ($\delta = 0.125$), orthorhombic $Sr_4Fe_4O_{11}$ ($\delta = 0.25$) and $Sr_2Fe_2O_5$ (or $SrFeO_{2.5}$, so-called Brownmillerite),[5] and recently discovered infinite layer compound $SrFeO_2$ ($\delta = 1$).[6] Two end members have been epitaxially grown on (001) perovskite substrates by PLD, followed by postgrowth annealing with strong oxidizing ($\delta = 0$) or reducing ($\delta = 1$) agents (i.e., ozone or CaH_2, respectively).[7−9] In all the studies, $SrFeO_{2.5}$ films are first prepared as precursors because the valence state of Fe^{3+} is robust in a typical range of growth conditions.[8] Nevertheless, the details of the epitaxial growth and structure of (001)-oriented $SrFeO_{2.5}$ films have not yet been reported. As for the physical properties, $SrFeO_3$ with the high spin Fe^{4+} ions has attracted much attention because of its metallicity and intriguing spin ordering structures: an antiferromagnetic long-range order with a helical spin structure below 134 K under atmospheric pressure and a ferromagnetic order above 400 K under pressures above 17 GPa.[10−12] Particular interest in the epitaxial growth of an (111)-oriented $SrFeO_{3-\delta}$ film also stems from the fact that the helicoid vector is parallel to the ⟨111⟩ direction.[10] To explore possible spintronics applications based on perovskite ferrates, controlling the heteroepitaxial growth of the (111)-oriented $SrFeO_{2.5}$ will provide a starting point.

In this paper, we have studied the PLD growth and structural properties of $SrFeO_{2.5}$ (SFO) films on $SrTiO_3$ (STO) (001) and (111) substrates. Such growth parameters as substrate temperature and oxygen partial pressure were fixed so that a two-dimensional layer-by-layer growth mode was achieved in the initial growth on both substrates, while we tuned the laser spot area, which has been recently found to influence the epitaxial structures significantly.[13] The films exhibit various types of multidomain structures depending on the growth direction and laser spot area, which is attributed to an epitaxial stabilization with a monoclinic structure derived from the original orthorhombic structure of bulk Brownmillerite. In order to explain the complicated manner of the epitaxial stabilization, we propose structure models, which in general provide a guidance to control the epitaxial

*To whom correspondence should be addressed. Electronic mail: aohtomo@imr.tohoku.ac.jp.

Published on Web 02/18/2010

Table 1. Lattice Parameters of $SrFeO_{2.5}$ Films

substrate	laser spot area	no. of domains	lattice constants/Å	tilt angles/deg			volume, V/Å^3	$V^{1/3}$/Å
				out-of-plane	in-plane	total		
(001)	small	4	3.905 (a_m) 3.989 (c_m)	1.4	0	1.4	60.81	3.932
	large	4	3.924 (a_m) 3.962 (c_m)	1.3	0	1.3	61.00	3.936
(111)	small	6 (3 [a])	2.299 (d_{111}) 1.607 ($d_{11\bar{2}}$)	0.3	0.6	0.9	61.71	3.952
	large	6	2.291 (d_{111}) 1.604 ($d_{11\bar{2}}$)	1.0	0.2	1.2	61.23	3.941

[a] Number of majority domains.

growth and structure of noncubic perovskites on (111) substrates.

2. Experimental Section

The SFO films were grown on atomically flat (001) and (111) surfaces of STO substrates (Shinkosha, Co., Ltd.) using a PLD system equipped with a semiconductor-laser-diode heater.[14] KrF excimer laser pulses (248 nm, 4 Hz) were focused on a target (a SFO ceramic tablet, 99.99% purity) with two different spot areas (0.35×0.10 cm^2 and 0.70×0.17 cm^2, hereafter referred as to "small" and "large" spot areas, respectively) at a constant fluence of 1 J/cm^2. The as-delivered (001) STO substrates were first ultrasonically cleaned in ethanol and acetone and then annealed in air at 1150 °C for 1 h to get TiO_2-terminated terrace and straight step structures. The STO (111) substrates were treated in hot water followed by cleaning in the organic solvents and annealing in air at 1050 °C for 1 h to obtain an atomically flat and Ti-terminated surface.[15] The substrates were loaded into an ultrahigh vacuum chamber and heated at 950 °C for 30 min in an oxygen partial pressure (P_{O_2}) of 1×10^{-6} Torr prior to growth. The PLD growth was performed at 830 °C in P_{O_2} = 0.8 mTorr with *in situ* monitoring of the reflection high-energy electron diffraction (RHEED) pattern. Some preparatory experiments were conducted to optimize the growth parameters so that clear RHEED intensity oscillations were observed. The film thickness was regulated in the range 75−260 nm. After the growth, the temperature was lowered at a rate of 20 °C/min, keeping P_{O_2} constant.

The surface morphology of the as-grown films as well as the annealed substrates was observed in air using atomic force microscopy (AFM, SPI-400, SII NanoTechnology). The film composition was analyzed for those grown on MgO (001) under the same conditions using a scanning electron microscope equipped with an electron probe microanalyzer (JED-2300F/JSM-6701F, JEOL) and the SFO target as a composition standard. Using four-circle X-ray diffraction (XRD, X'pert MRD, PANalytical) with Cu Kα radiation (λ = 1.541838 Å), we characterized the film structures. All the results are shown and discussed for the four samples listed in Table 1.

3. Results and Discussion

Figure 1a and c shows typical RHEED intensity oscillations recorded during the initial growth of SFO films on (001) and (111) STO substrates, respectively, indicating a two-dimensional layer-by-layer growth mode. It is found that the persistency of the oscillations was quite different for substrate orientations. The oscillation amplitude as well as reflected intensity damped quickly for the (111) case, indicating a transition to a three-dimensional growth mode, perhaps at the initial stage of domain formation. The difference in the growth mode is reflected in the surface morphologies, as shown in the inset AFM images. The (001)-oriented film displays the original atomically flat surface structure of the substrate, including 0.4-nm-high steps, whereas the surface of the (111) film is rough, exhibiting small triangular islands. We notice that (111)-oriented perovskite epitaxy is often *uneasier*

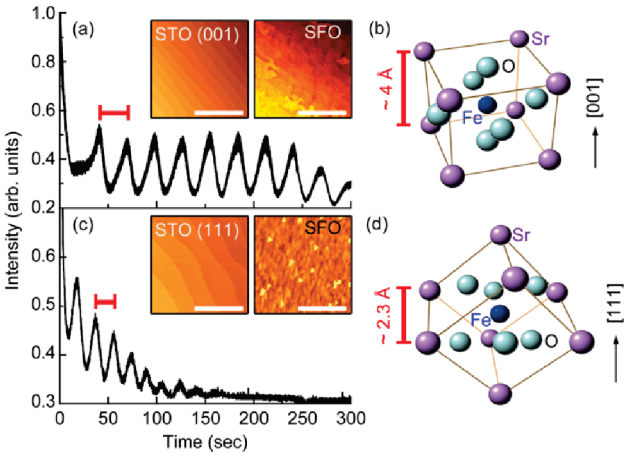

Figure 1. RHEED intensity oscillations for the specular beam during the initial growth of $SrFeO_{2.5}$ films on (a) (001) and (c) (111) $SrTiO_3$ substrates with small spot area of ablation laser. Schematics of growth unit cells of the (b) (001)- and (d) (111)-oriented films, showing that each single oscillation corresponds to a thickness of ~4 Å and ~2.3 Å, respectively. The insets of parts a and c depict AFM images of the substrates (left) and films (right); scale bars are 1 μm, and color codes are ~7 nm in height.

than that for (001)- and (110)-oriented ones, to which a possible origin of our particular case will be discussed in terms of disordered atomic structures at heterointerfaces. We estimated the growth rate from the total film thickness measured by a surface profilometer to find that the thicknesses corresponding to one oscillation were 0.4 and 0.23 nm on (001) and (111) substrates, respectively, which is consistent with the charge-neutral formula unit cells along each orientation (Figure 1b and d). The growth rate was found to be independent of laser spot area [3.5×10^{-3} nm/pulse and 3.2×10^{-3} nm/pulse on the (001) and (111) surfaces, respectively].

The composition of cations in all the films was confirmed to be identical to that of the target regardless of laser spot area. Wide-range XRD scans along the out-of-plane reflections revealed that single phase SFO has been formed without any secondary phase. Sharp film peaks were observed near substrate peaks, as indicated by arrows in Figure 2. Tuning laser spot area small resulted in expansion of lattice parameters for both orientations. As for the (111)-oriented film grown with small spot area, no apparent film peak was seen when the pattern was taken with aligning to the 222 STO reflection (solid line in the upper panel of Figure 2b); however, a clear peak appeared, when aligned to the 222 SFO reflection (dotted line). This result indicates that the film plane tilts with respect to the substrate plane, which was not seen in the other samples. We discuss the details of this tilt in the next few paragraphs.

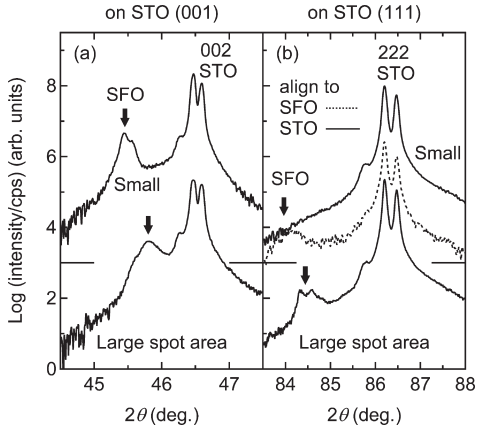

Figure 2. X-ray diffraction patterns for $SrFeO_{2.5}$ films grown on (a) (001) and (b) (111) $SrTiO_3$ substrates. The upper and lower curves in each panel were taken for films grown with small and large spot area, respectively. All the patterns were taken by aligning to substrate reflections, except for the one shown by a dotted line (aligning to film reflection). The arrows depict the positions of the film peaks.

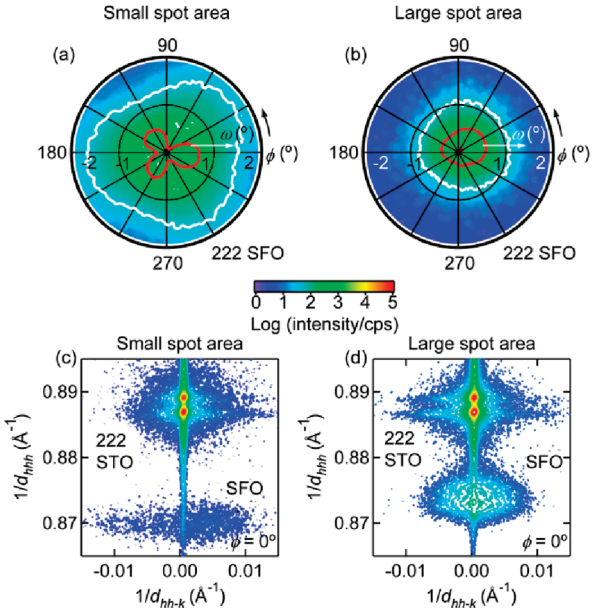

Figure 3. X-ray pole figures (along the ω- and ϕ-axes) of 222 $SrFeO_{2.5}$ reflections for films grown on (111) $SrTiO_3$ (STO) substrates with (a) small and (b) large spot area. Red and white curves display contour lines leveled at 50% and 10% of peak intensity of the film reflections, respectively. (c and d) Reciprocal space maps around 222 STO reflections taken at $\phi = 0°$ [incidence parallel to the $(1\bar{1}0)$ STO plane] for the films shown in parts a and b, respectively.

In order to evaluate tilt angle and direction, we measured pole figures ($\omega-\phi$ scans) for 222 SFO reflections, which are shown in Figure 3a and b for films grown with small and large spot area, respectively. The former sample clearly showed 3-fold peaks located at $\omega \sim 0.5°$ and $\phi \sim 0$, 120, and 240°, indicating that the dominant tilting directions coincide with the $\langle 11\bar{2} \rangle$ directions. Note that a contour at the half-maximum intensity is shown by a red solid line. In addition, there can be seen tails at $\phi \sim 60$, 180, and 300°, as highlighted by a white solid line (contour level of 10%). Such predominant tilting configurations should be attributed to a crystallographic origin, as will be explained later. As for the films grown with large spot area, only a single pole centered at a narrow region was observed. It is worth mentioning that while we took the pole figures, there have been seen sharp and high intensity peaks at the centers. They were actually associated with long tails of the substrate peak (i.e., critical truncation rods along *hhh*) but not with film components, as shown in reciprocal lattice maps around 222 STO reflections (Figure 3c and d). We notice that slightly asymmetric shapes of the peaks seen in pole figures are artifacts due to misalignment of the goniometer and/or asymmetric ϕ-scan geometry (an X-ray beam with an oval projection was exposed on rectangular-shaped samples). In fact, the 222 SFO reflection in Figure 3d shows a symmetric feature.

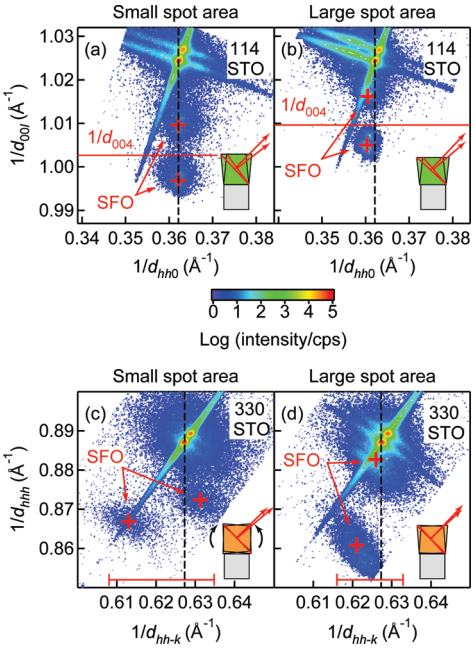

Figure 4. Reciprocal space maps around 114 $SrTiO_3$ (STO) reflections for films grown on (001) STO substrates with (a) small and (b) large spot area, and around 330 STO reflections for films grown on (111) STO substrates with (c) small and (d) large spot area. The inset at the right bottom in each panel depicts schematic domain structures. Crossing bars (red) indicate two splitting peaks of the film reflections, and vertical dashed lines (black) are guides for the substrate peak positions. The red horizontal lines shown in parts a and b correspond to the positions of 004 $SrFeO_{2.5}$ reflections. The bars shown at the bottom of parts c and d are referred to in the text.

To understand the origin of the tilt, we measured reciprocal space maps around asymmetric STO reflections. As shown in Figure 4a and b, (001)-oriented films exhibited two split peaks along 00*l* for 114 SFO reflections, which at first sight may appear due to the presence of a twin structure, as often seen in the orthorhombic high-T_c superconducting cuprites.[16] When maps were taken for *h*0*l* and 0*kl* reflections, however, these splittings appeared with three peaks equally spaced along 00*l* (data not shown). In addition, given the fact that the centers of split peaks were always located at the positions of symmetric 00*l* reflections (for example, indicated by red crossing bars and lines in Figure 4a and b), these features are consistent with the presence of four monoclinic domains observed for a (001)-oriented $SrRuO_3$ film on $SrTiO_3$.[17] This situation is schematically drawn for a pair of mirror domains in insets. The tilt angles estimated from split peak positions were 1.4° and 1.3° for the films grown with small and large spot areas, respectively. Different *c*-axis lattice parameters, induced by change of laser spot area (Figure 2a), can be understood in terms of

the shift of the *a*-axis lattice parameters. The film grown with small (large) spot area was strained (partially relaxed), exhibiting a value identical to (longer than) that of STO along the *a*-axis, which is responsible for the longer (shorter) value along the *c*-axis. As a result, the unit cell volumes (V) in both films are almost identical (see Table 1). Thus, it is concluded that tuning laser spot area merely affects the strain relaxation dynamics but not much the oxygen nonstoichiometry in the films.

Similar data were obtained for the films grown on (111) STO substrates (Figure 4c and d), but the splitting directions were rather diagonal, neither vertical nor horizontal, such as one may expect on the basis of the results shown in Figures 3a and 4a and b. The diagonal tilt is due to different degrees of tilt divided into vertical and horizontal directions; in other words, neither the out-of-plane nor in-plane lattices are restricted to be parallel to those of substrate. The predominant tilt directions were in-plane for film with small spot area and out-of-plane for film with large spot area. The sums of the tilt angles in both directions were approximately 1° in both films, and the unit cell volume was found to be slightly larger for film with small spot area. It is worth noting that components of vertical splitting must have appeared in symmetric reflections. This is true for film with small spot area (Figure 3c) that display two different intensities for the majority (right spot) and minority domains (left spot). However, only a single broad peak is seen for films with large spot areas due to small peak separation (Figure 3d). The ranges of visible 222 SFO reflections along the horizontal axis in Figure 3c and d are shown by red bars at the bottom of Figure 4c and d to compare different situations. The impact of laser spot area on the epitaxial structure of (111)-oriented films is summarized as follows: the predominant tilt direction shifts from in-plane to out-of-plane with increasing laser spot area, and meanwhile the number of domains tends to increase from three to six.

Having established variant tilting and domain configurations resulting from monoclinic structure, we turn now to discuss the origin. The monoclinic structure is directly derived from the original orthorhombic structure of bulk Brownmillerite. Figure 5a shows their relationship as well as a triangular prism cell representing an epitaxial unit cell on (111) substrates. (Note that such a large unit cell of Brownmillerite is caused by the ordering of oxygen vacancies in the perovskite framework, with one oxygen-deficient $SrFeO_2$ row alternating with one fully occupied $SrFeO_3$ row along the a_o-axis.[18]) The parent cell is divided into eight fundamental perovskite blocks having a cell volume of 61.02 Å^3, one of which is indicated with the green shade. In this configuration, the original lattice parameters (a_o = 5.6685, b_o = 15.5824, and c_o = 5.5265)[19] are reduced to $a_m = c_m = (a_o c_o/2)^{1/2}$ = 3.9577 and $b_m = b_o/4$ = 3.8956. The obtuse angle in the $a_m c_m$-plane (β) is 91.45°. Two different planes, rectangle (patch) and parallelogram (crosshatched), have averaged lattice mismatches of 0.6 and 1.4% to the STO (001) plane, respectively. Therefore, the former must face down to the substrate, while the latter comprises a side plane. As a natural consequence, the c_m-axis of SFO tilts toward the 4-fold *a*- and *b*-axes of STO by ~1.5° and four mirror-variant domains are formed (Figure 5b). The tilt angles as well as cell volumes for films grown on (001) substrates are in good agreement with those obtained with this model.

Similar arguments are possible to account for the case of the (111) substrate. There are two possible planes to be faced to

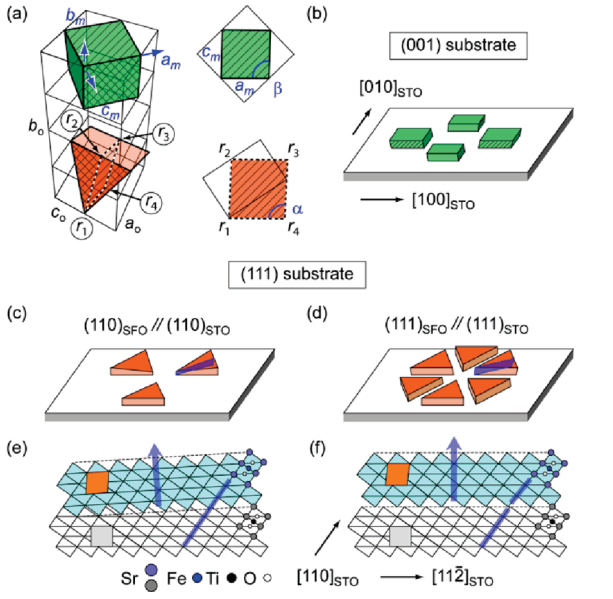

Figure 5. Schematic epitaxial structure model of $SrFeO_{2.5}$ (SFO) films. (a) Monoclinic and triangular prism unit cells shown with the original orthorhombic unit cell, where the $a_m b_m$-plane and a triangular plane (crosshatch) are thought to face the (001) and (111) planes, respectively. In these configurations, film cross sections are comprised of the $a_m c_m$-plane and an internal mirror plane of the triangular prism indicated with $r_1 \sim r_4$ (hatch), both of which are parallelograms with β and α equal to ~91.5°. These tilts will give rise to multidomain structures for the films grown on (b) (001) and (c, d) (111) substrates. (e, f) Possible atomic arrangements at the interface (shaded cross sections in parts c and d). Semitransparent bars and arrows depict the A-site atom column along the [110] direction and the SFO [111] direction, respectively.

the substrate, the one of them giving smaller lattice mismatch (0.4%) is drawn with an isosceles triangle (crosshatched) situated on an orange-shaded triangular prism cell in Figure 5a. Another triangular plane shares one edge with an orthorhombic cell along the a_o-axis (lattice mismatch 1.3%). Considering a cross section of the unit cell, we choose an internal mirror-symmetry plane, of which corners are indicated with $r_1 \sim r_4$, because the reciprocal space maps shown in Figure 4c and d have been measured parallel to this plane. One of its interior angles (α) is calculated to be 91.54°; therefore, the situation is very similar to the case of the (001) substrate. Two ideal cases can be considered as schematically drawn in Figure 5c–f. In the first case, the (111) film plane is tilted toward the 3-fold $\langle 11\bar{2} \rangle$ direction of STO so that the (110) planes of film and substrate become parallel to each other. The opposite situation is represented in the second case except for allowing formation of mirror variant domains. The experimentally observed epitaxial relationships strongly support these models for the following reasons. First, predominant tilting configurations (directions and angles) agree with each case. Second, the number of the majority domains in the film with the small spot area is three. In addition, the triangular islands seen in the AFM image for the film with the small spot area (see the inset of Figure 1c) are preferentially oriented to the $\langle 11\bar{2} \rangle$ directions, just like those shown in Figure 5c. Third, the presence of mirror variant domains manifests itself in vertical splitting of the asymmetric reflection observed for films with large spot area, being analogous to (001)-oriented films. This also explains the appearance of minority domains in films with small spot areas. The formation of mirror variant

domains has been observed for monoclinic oxide films grown on cubic (111) substrates.[20]

Our discussion is so far restricted to the situations at room temperature. According to the temperature dependence of lattice parameters reported for SFO and STO,[19,21] the model mentioned above holds its relevance at temperatures up to ~900 °C, above which SFO transforms to cubic due to disorder in oxygen vacancy sites. However, we note that asymmetry in unit planes (crosshatched rectangle and isosceles triangle) has been smeared in the films, meaning that for all the samples the in-plane lattice constants along different axes were identical to each other. Although the origin is unclear, it may be attributed to the disordering of oxygen vacancies, since films were grown under the conditions in the vicinity of the structural transition.

4. Conclusion

Using PLD, we have studied the heteroepitaxial growth of oxygen deficient SFO perovskite films on STO (001) and (111) substrates and their epitaxial structures as a function of laser spot area. The models explaining the observed epitaxial structures are developed, which we believe provide important guidelines for the preparation and stabilization of noncubic perovskite heterostructures having versatile functionalities. Our findings are summarized as follows. (1) The change of laser spot area significantly alters lattice parameters along different axes, while keeping the unit cell volume nearly constant. (2) The films with both orientations were stabilized with the monoclinic structure derived from the bulk orthorhombic structure. (3) Different orientations of the monoclinic lattice appear with different numbers of mirror variant domains. (4) In the case of the (111) substrate, the predominant tilting directions of the [111] axis shift from in-plane to out-of-plane with increasing laser spot area, giving rise to a higher degree of orientation along the growth direction, whereas the number of domains tends to increase from three to six. This compromise can be overcome by the use of a miscut substrate, as demonstrated for "domain engineering" of rhombohedral $BiFeO_3$ films grown on (001) STO.[22]

Acknowledgment. S.C. acknowledges financial support from the Global COE Materials Integration Program, Tohoku University. and the Japan Society for the Promotion of Science (JSPS). We thank Y. Iwasaki for his technical assistance with XRD measurements.

References

(1) (a) Pickett, W. E. *Rev. Mod. Phys.* **1989**, *61*, 433–512. (b) Tokura, Y. *Physica C* **1991**, *185*, 174–179. (c) Dagotto, E. *Rev. Mod. Phys.* **1994**, *66*, 763–840. (d) Ramirez, A. P. *J. Phys.: Condens. Mater.* **1997**, *39*, 8171–8199. (e) Coey, J. M. D.; Viret, M.; von Molnar, S. *Adv. Phys.* **1999**, *48*, 167–293. (f) Ramesh, R.; Spaldin, N. A. *Nat. Mater.* **2007**, *6*, 21–29.

(2) (a) Ohtomo, A.; Muller, D. A.; Grazul, J. L.; Hwang, H. Y. *Nature* **2002**, *419*, 378–380. (b) Lee, H. N.; Christen, H. M.; Chisholm, M. F.; Rouleau, C. M.; Lowndes, D. H. *Nature* **2005**, *433*, 395–399.

(3) (a) Kobayashi, K.-I.; Kimura, T.; Sawada, H.; Terakura, K.; Tokura, Y. *Nature* **1998**, *395*, 677–680. (b) Manako, T.; Izumi, M.; Konishi, Y.; Kobayashi, K.-I.; Kawasaki, M.; Tokura, Y. *Appl. Phys. Lett.* **1999**, *74*, 2215–2217.

(4) Eason, R. *Pulsed Laser Deposition of Thin Films: Application-Led Growth of Functional Materials*; John Wiley & Sons, Inc.: Hoboken, NJ, 2007.

(5) Takeda, Y.; Kanno, K.; Takeda, T.; Yamamoto, O.; Takano, M.; Nakamura, N.; Bando, Y. *J. Solid State Chem.* **1986**, *63*, 237–249.

(6) Tsujimoto, Y.; Tassel, C.; Hayashi, N.; Watanabe, T.; Kageyama, H.; Yoshimura, K.; Takano, M.; Ceretti, M.; Ritter, C.; Paulus, W. *Nature* **2007**, *450*, 1062–1065.

(7) Hayashi, N.; Terashima, T.; Takano, M. *J. Mater. Chem.* **2001**, *11*, 2235–2237.

(8) Yamada, H.; Kawasaki, M.; Tokura, Y. *Appl. Phys. Lett.* **2002**, *80*, 622–624.

(9) Inoue, S.; Kawai, M.; Shimakawa, Y.; Mizumaki, M.; Kawamura, N.; Watanabe, T.; Tsujimoto, Y.; Kageyama, H.; Yoshimura, K. *Appl. Phys. Lett.* **2008**, *92*, 161911.

(10) (a) Takeda, T.; Yamaguchi, Y.; Watanabe, H. *J. Phys. Soc. Jpn.* **1972**, *33*, 967–969. (b) Oda, H.; Yamaguchi, Y.; Takei, H.; Watanabe, H. *J. Phys. Soc. Jpn.* **1977**, *42*, 101–106.

(11) Lebon, A.; Adler, P.; Bernhard, C.; Boris, A. V.; Pimenov, A. V.; Maljuk, A.; Lin, C. T.; Ulrich, C.; Keimer, B. *Phys. Rev. Lett.* **2004**, *92*, 037202.

(12) Kawakami, T.; Nasu, S.; Kuzushita, K.; Sasaki, T.; Morimoto, S.; Yamada, T.; Endo, S.; Kawasaki, S.; Takano, M. *J. Phys. Soc. Jpn.* **2003**, *72*, 33–36.

(13) (a) Ohnishi, T.; Lippmaa, M.; Yamamoto, T.; Meguro, S.; Koinuma, H. *Appl. Phys. Lett.* **2005**, *87*, 241919. (b) Song, J. H.; Susaki, T.; Hwang, H. Y. *Adv. Mater.* **2008**, *20*, 2528–2532.

(14) Ohashi, S.; Lippmaa, M.; Nakagawa, N.; Nagasawa, H.; Koinuma, H.; Kawasaki, M. *Rev. Sci. Instrum.* **1999**, *70*, 178–183.

(15) Chang, J.; Park, Y.-S.; Kim, S.-K. *Appl. Phys. Lett.* **2008**, *92*, 152910.

(16) Raveau, R.; Michel, C.; Hervieu, M.; Groult, D. *Crystal Chemistry of High T_c Superconducting Copper Oxides*; Springer-Verlag: Berlin, 1991.

(17) Saito, K.; Ulyanenkov, A.; Grossmann, V.; Ress, H.; Bruegemann, L.; Ohta, H.; Kurosawa, T.; Ueki, S.; Funakubo, H. *Jpn. J. Appl. Phys.* **2006**, *45*, 7311–7314.

(18) Rao, C. N. R.; Raveau, B. In *Transition Metal Oxides: structure, properties, and synthesis of ceramic oxides*, 2nd ed.; John Wiley & Sons, Inc.: New York, 1998; Part I, pp 46−49.

(19) Schmidt, M.; Campbell, S. J. *J. Solid State Chem.* **2001**, *156*, 292–304.

(20) (a) Sumi, A.; Kim, Y. K.; Oshima, N.; Akiyama, K.; Saito, K.; Funakubo, H. *Thin Solid Films* **2005**, *486*, 182–185. (b) Hiraga, H.; Fukumura, T.; Ohtomo, A.; Makino, T.; Ohkubo, A.; Kimura, H.; Kawasaki, M. *Appl. Phys. Lett.* **2009**, *95*, 032109.

(21) Biegalski, M. D.; Haeni, J. H.; Trolier-McKinstry, S.; Schlom, D. G.; Brandle, C. D.; Ven Graitis, A. J. *J. Mater. Res.* **2005**, *20*, 952–958.

(22) Jang, H. W.; Ortiz, D.; Baek, S.-H.; Folkman, C. M.; Das, R. R.; Shafer, P.; Chen, Y.; Nelson, C. T.; Pan, X.; Ramesh, R.; Eom, C.-B. *Adv. Mater.* **2009**, *21*, 817–823.